The published version of the paper "Laura Ierimonti, Luca Caracoglia, Ilaria Venanzi, Annibale Luigi Materazzi, Investigation on life-cycle damage cost of wind-excited tall buildings considering directionality effects, Journal of Wind Engineering and Industrial Aerodynamics, Volume 171, 2017, Pages 207-218, ISSN 0167-6105" is available at: https://doi.org/10.1016/j.jweia.2017.09.020

Investigation on life-cycle damage cost of wind-excited tall buildings considering directionality effects

Laura Ierimonti[a,b,1,*], Luca Caracoglia[b], Ilaria Venanzi[a], Annibale Luigi Materazzi[a]

[a] *Department of Civil and Environmental Engineering, University of Perugia. Via G. Duranti, 93 - 06125 Perugia, Italy.*
[b] *Department of Civil and Environmental Engineering, Northeastern University, 360 Huntington Avenue, Boston, MA 02115, USA.*

Abstract

Life-cycle cost analysis (LCCA) can be efficiently used to quantify wind-induced damage on a tall building. The LCCA selects an "optimal" design solution by minimizing over structural lifetime the total cost (construction, maintenance and repair). Being based on the *Pacific Earthquake Engineering Research* equation, the LCCA relates the expected cost over the lifetime of the structure to the probability of exceeding specific damage levels. It also accounts for potential sources of uncertainty, such as variability in wind load intensity, directionality, structural properties, damage model estimation, etc. This paper proposes a LCCA methodology that evolves from the approach used in seismic engineering to numerically examine non-structural damage

*Corresponding author. Department of Civil and Environmental Engineering, University of Perugia. Via G. Duranti, 93 - 06125 Perugia, Italy. phone: +39 075 585 3908; fax: +39 075 585. 3897

Email addresses: ierimonti@strutture.unipg.it (Laura Ierimonti), lucac@coe.neu.edu (Luca Caracoglia), ilaria.venanzi@unipg.it (Ilaria Venanzi), annibale.materazzi@unipg.it (Annibale Luigi Materazzi)

[1] J-1 Visiting Research Assistant at Northeastern University in 2016 on temporary leave from the University of Perugia, Italy

probability and predict maintenance costs on tall buildings by incorporating information on aerodynamic loads measured on a reduced-scale model in wind tunnel. The final objective is to provide an efficient simulation procedure, which simultaneously accounts for stochastic characterization of wind load intensity and direction.
Keywords: Life-cycle cost analysis; wind load; tall buildings;
non-structural damage; wind direction.

---

1. Introduction

Wind-exposed tall buildings can experience damage to non-structural components during their lifetime. Non-structural damage can pertain to partition walls, installations, ceilings, façades. For example, damage to façades can be induced by strong winds producing disproportionate lateral inter-story drifts, accelerations, large pressures loads at specific locations of the structural envelope or by impact of wind-borne debris. Only in the case of occurrence of very strong wind events like tornadoes, the building can experience structural damage and collapse of structural members (LaFave et al., 2016). As confirmed by forensic engineering investigations after extreme wind hazards, adequate initial design usually avoids altogether such a problem in the case of engineered tall buildings; consequently, most attention is usually devoted to non-structural damage.

In order to assess life-cycle losses in tall buildings due to non-structural damage, an appropriate methodology is required. One such methodology that has gained attention in recent years is the life-cycle cost analysis (LCCA). The LCCA can estimate the total costs of a structure accounting for the

effects of uncertainties involved in the design that cannot be neglected (Venanzi, 2015; Venanzi et al., 2015, 2014). Moreover the LCCA can account for structural deterioration, structural and non-structural damage, maintenance and repair interventions (Lagaros, 2007; Okasha and Frangopol, 2011). The LCCA is a well established process in earthquake engineering (Aslani and Miranda, 2005; Liu et al., 2004; Mitropoulou et al., 2011; Wen and Kang, 2001) while in wind engineering considerable efforts are still needed to improve applicability of the methods and models.

In Ciampoli et al. (2011) a performance-based design approach for wind engineering is formalized for the first time. In Ciampoli and Petrini (2012); Pozzuoli et al. (2013) the method is employed to assess the risk of exceeding serviceability limit states in tall buildings subjected to wind load. In Spence and Kareem (2014) the research focus is devoted to the definition of site-specific wind hazard models, derivation of suitable fragility functions as well as of consequence functions that can rationally assess damage and monetary losses. Recent works concerning life-cycle cost analysis of structures under wind loads presented relevant contributions in this field by adapting several concepts and methods from the seismic engineering field. Cui and Caracoglia (2015, 2016); Seo and Caracoglia (2013) propose a numerical framework to estimate the life-cycle monetary losses due to wind-induced damage on long-span bridges and tall buildings, respectively. A risk design optimization method for optimizing life-cycle costs and functionality of tall buildings is proposed in Li and Hu (2014). A general framework for the LCCA of tall buildings subjected to both seismic and wind excitation is discussed in Venanzi et al. (2017). Minimization of life-cycle cost is also explored for the

optimal design of tall buildings under wind load (Huang et al., 2016) and equipped with control devices (Beck et al., 2014; Wang et al., 2016). In all the methods briefly reviewed above, the monetary loss assessment is based on the numerical estimation of the *Pacific Earthquake Engineering Research* (PEER) equation, which allows computing the probability of exceeding a pre-defined damage threshold and, consequently, *intervention and repair cost* (Ramirez et al., 2012; Ramirez and Miranda, 2012) by accounting for several uncertainty sources in the load and damage model. In a general framework application, the model should first consider the uncertainty related to wind load characterization due to the inherent stochastic nature of the wind load, including both wind speed and direction. Second, it must account for uncertainty in the aerodynamic models and structural properties of the building, which are relevant to the response estimation.

Capitalizing from the existing literature results and recent advancements of models and methods, the main objective of this study is to provide a general and computationally efficient procedure that relates the probability of exceeding a specific non-structural damage state to the intervention and repair cost of a wind-sensitive structure by considering the stochastic nature of the loads. In this first implementation of the procedure, the fundamental sources of uncertainty are considered such as those associated with aerodynamic loads, wind load intensity and directionality. This study makes use of a benchmark building structure, wind tunnel load data and full-scale wind speed and direction data records. By accounting for the probability distribution of the wind direction, the life-cycle cost is evaluated as a function of both time and building's orientation angle. The results of the LCCA procedure

provide useful information to the designers and assistance to the selection of the orientation that minimizes the total life-cycle cost. Although the orientation of a tall building in an existing urban context could be significantly constrained by the presence of neighboring buildings, by architectural and functionality issues, the primary role of building orientation in a performance-based design setting has been clearly emphasized by researchers [e.g., Jain et al. (2001)]. Without loss of generality the present paper examines the influence of wind exposure of a specific site on building's design in order to find the best cost-saving structural solution.

The main features and novel features of the proposed procedure are:

1. contrary to most literature studies concerning LCCA of wind-exposed tall buildings, which assume the intervention and repair cost to be directly associated with the probability of exceeding a pre-selected limit state at a global or floor level, the cost is indirectly related to the probability of exceeding a damage state obtained by incorporating specific structural fragility functions at the component level (e.g., window glass cracking); the damage model is derived for tall, slender, low-frequency structures which are primarily sensitive to dynamic resonant effects, such as interstory drift, rather than direct pressure loads or wind-borne debris (i.e., conceived for a first application example outside of the hurricane-prone regions in the United States);
2. the procedure is computationally efficient since wind tunnel high-frequency force balance (HFFB) records are used and converted to generalized forces along with their uncertainty, enabling the analysis in the frequency domain;

3. structural damage, intervention and repair costs are separately considered and accumulated along both principal lateral deformation planes of the building;
4. the effect of wind directionality and the building orientation at a specific site are taken into account in the computation of the expected life-cycle costs.

Uncertainty in the wind load estimation is examined and used to assess the probability distributions of the damage-related response components by splitting the wind tunnel records in several segments corresponding to independent realizations of the stochastic load process.

The rest of the paper is organized as follows. The wind damage and loss analysis model is presented in Section 2. The case study is described in Section 3. Section 4 presents the numerical results and, finally, Section 5 concludes the paper.

2. Wind damage and analysis model

2.1. Load and response model: motivation and assumptions

The model assumes that, as damage is predominantly non-structural and occurs on secondary structural elements, the main resisting structural system remains linear during the wind event and the response is dominated by the fundamental lateral vibration modes. If the main lateral resisting system is symmetrical and mass eccentricity is small, torsional effects can be neglected in the case of intervention-cost analysis, as suggested by previous studies (Caracoglia, 2014; Cui and Caracoglia, 2015, 2016). This hypothesis is therefore used in the first implementation of the proposed methodology,

which analyzes the lateral dynamic translation of the building floors only. It is worth noticing that the the effect of torsion may possibly affect the life cycle cost results because the consequent horizontal and vertical peak shear strain can act in combination with the translational response of the building, especially for façade elements at the corners, (Charney and Johnson, 1986; Griffis, 1993). These complex aspects should possibly be treated separately as a function of the specific technology of the façade considering the maximum allowable relative movement between the two bonded surfaces of a curtain wall system. They are, however, beyond the main objectives of this study, which primarily describes derivation and implementation of the procedure, but will be readily considered in future developments. The damage analysis is initially conducted in each primary orthogonal lateral deflection planes of the building separately due to the specific benchmark building geometry that was selected; the results along the two directions are subsequently combined to obtain the cumulative effect in both directions. Hence a simplified model is proposed in order to evaluate the influence of the horizontal peak response due to the building torque in combination with the lateral displacement.

2.2. Load and response model: summary description and derivation of principal equations

In this sub-section the fundamental equations of the model are provided for the sake of conciseness as they are derived from a standard frequency-domain approach; the reader is referred to standard approaches used in the wind engineering literature for more details [for example, refer to the description presented in Cui and Caracoglia (2015)]. In order to limit the computational effort required by the LCCA procedure while still preserving adequate

estimation accuracy, the wind loads are represented as time-dependent generalized forces and the structural analysis is carried out in the frequency domain (Caracoglia, 2014). The generalized loads of the fundamental lateral modes, associated with the turbulent wind pressure loads on the building's surface, are needed. These quantities can be directly evaluated from wind tunnel data via conventional HFFB tests or can be obtained by integrating synchronous wind pressure measurements.

A key point of the procedure relies on the examination and indirect estimation of wind loading uncertainty by exploiting information derived from the time histories of the experimental pressure loads, measured in wind tunnel by HFFB. In order to examine the measurement uncertainty, a long HFFB record of the total base bending moments is divided in $i = 1, .., N$ segments of equal time duration Δt. Each i^{th} segment is treated as an independent realization of the generalized force which is labeled as $F_{Q_{i,k}}(t)$. The quantity t indicates time ($0 \leq t \leq T$) and $k = \{x, y\}$ are the principal orthogonal directions of the building. The generalized lateral force $F_{Q_{i,k}}(t)$, from which the structural response is evaluated, can be written as:

$$F_{Q_{i,k}}(t) = \int_0^H f_{i,k}(z,t)[\Phi_k(z)]\mathrm{d}z = \int_0^H f_{i,k}(z,t)\left[\frac{z}{H}\right]\mathrm{d}z = \frac{1}{H}\int_0^H f_{i,k}(z,t)\mathrm{d}z \tag{1}$$

In the previous equation H is the building height, $f_{i,k}(z,t)$ is the i^{th} realization of the experimental aerodynamic force per unit height in the $k = \{x, y\}$ direction calculated at height z (for example by local pressure integration); $\Phi_k(z)$ is the fundamental mode shape in the k direction. In this first application of the procedure, $\Phi_k(z) = \frac{z}{H}$ is assumed to vary linearly along the height. In principle, it is possible to account for nonlinear mode shapes (i.e.,

for the influence of higher modes), by adopting the following exponential form $\left[\frac{z}{H}\right]^{\gamma}$ with $\gamma > 1$.

After normalization, the generalized force becomes:

$$\hat{F}_{Q_{i,k}}(t) = \frac{F_{Q_{i,k}}(t)}{1/2 \rho V_{ref}^2 H D} \tag{2}$$

where ρ is the air density; V_{ref} is the reference value of the mean-wind speed (ten-minute average) at the roof height; D is a reference lateral-horizontal dimension of the structure.

By following standard approaches, after removal of the mean load component from the fluctuating aerodynamic loads and some manipulation, the previous equation may be converted to frequency domain to obtain the generalized force spectrum. The following normalized generalized force spectrum is adopted in the numerical analysis:

$$nS_{\hat{F}_{Q_{i,k}}}(n) = \frac{nS_{F_{Q_{i,k}}}(n)}{(1/2 \rho V_{ref}^2 H D)^2} \tag{3}$$

where n is the frequency and $S_{F_{Q_{i,k}}}$ is the power spectrum of the i^{th} experimental realization of the generalized force in the k^{th} direction.

The response in each principal lateral direction of the building with uncoupled uni-planar mode shapes [$\Phi_x(z)$ oriented along x lateral building direction and $\Phi_y(z)$ along y lateral building direction] can be determined independently through the fundamental frequency-domain modal response analysis as a first approximation when the response is dominated by the resonant effect related to the fundamental lateral modes of the building. The power spectrum of the generalized wind load is consequently combined with the dynamic response in each modal coordinate by neglecting inter-modal

coupling to find the peak dynamic response of the full-scale structure in the frequency domain. For this purpose the spectral analysis and Davenport Chain (Davenport, 1964) may be employed, treated independently in the two principal directions x and y as the cost accumulation can also be conveniently evaluated separately first and later cumulated as described in a later section). Under the assumption of a stationary multi-variate Gaussian process valid for both wind force and structural response, the maximum lateral displacement $D_{i,k}$ of the structure in the k^{th} principal direction, evaluated using wind spectral information from the i^{th} wind tunnel realization of the load, is found as follows:

$$D_{i,k} = \bar{D}_{i,k} + g_{i,k} \cdot \sigma_{D,i,k} \tag{4}$$

where $\bar{D}_{i,k}$ is the mean response, $\sigma_{D,i,k}$ is its standard deviation, and $g_{i,k}$ is the peak factor computed in accordance with the structural response spectrum and Davenport's theory. It is noted that both $\bar{D}_{i,x} = \bar{X}_i$ and $\bar{D}_{i,y} = \bar{Y}_i$ can be different from zero, either because the mean-wind incidence angle does not usually coincide with one of the principal lateral deformation planes or because of shape asymmetry and influence of surrounding buildings on the loads that lead to non-zero across-wind mean response.

2.3. Damage analysis

The probability of exceeding a pre-selected level of damage can be computed in accordance with the principles of the PEER approach (Cornell and Krawinkler, 2000), recently adopted in wind engineering with some adaptations from seismic engineering.

Since the wind load is usually a function of the mean-wind direction, the probability of exceeding a specific level of damage depends on the building orientation vs. mean-wind incidence angle. Figure 1 illustrates a schematic view of the plan and of the elevation of a generic tall building with the indication of the angle δ, denoting the building orientation with respect to the North direction, and the angle θ, characterizing the relative mean-wind incidence angle measured from the reference building axis x of the local coordinate system. The angle θ is used as a reference measure of direction, compatible with the building model orientation in standard wind tunnel experiments. The sign convention for δ and θ is considered positive according to a clockwise rotation. For the purpose of the analysis the mean-wind direction angle is defined as the summation between the building orientation angle δ and the angle θ, e.g. $(\theta + \delta)$, in the interval between 0° and 360°:

$$(\theta+\delta) = \begin{cases} (\theta+\delta) & \text{if } (\theta+\delta) < 360^o, \\ (\theta+\delta) - 360^o & \text{if } (\theta+\delta) \geq 360^o. \end{cases} \tag{5}$$

For the sake of clarity with reference to Figure 1a), $(\theta + \delta) = 0^\circ$ corresponds to a Northerly wind.

The original formulation of the convolution integral (Ciampoli et al., 2011; PEER-TBI, 2010) is modified in this study to evaluate the annual damage probability in the k direction associated with limit state j and accounting for the mean-wind incidence angle δ as follows:

$$P_j^k(\delta) = \int\int\int\int P[DS_j|EDP] f[EDP|IM,SP,IP] \\ f(IP|IM,SP) f[IM(\delta)] f(SP) \mathrm{d}(EDP) \mathrm{d}(IP) \mathrm{d}(IM) \mathrm{d}(SP) \tag{6}$$

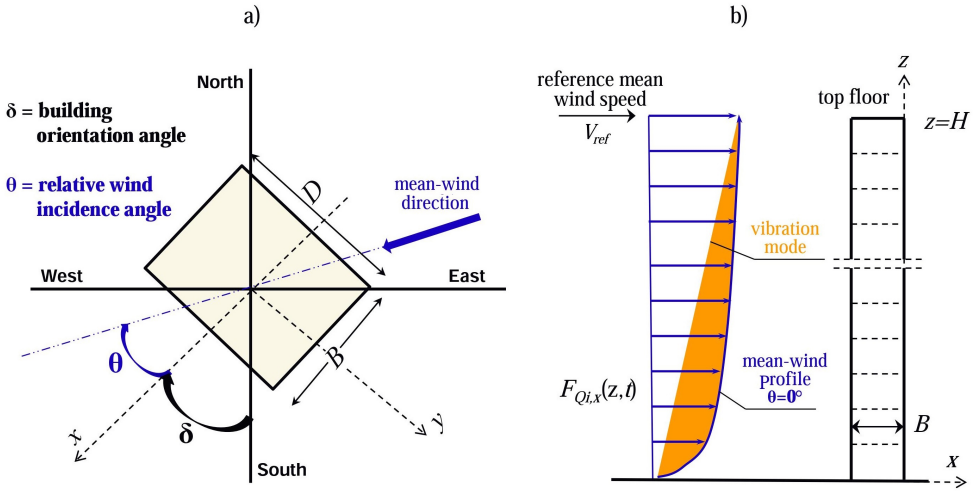

Figure 1: Schematic plan view and elevation of the benchmark tall building.

where DS_j is the jth damage state; EDP is the vector collecting the engineering demand parameters (i.e. structural response components) inducing the damage; IM is the vector of the intensity measure; SP is the vector of the parameters characterizing the structural system; IP is the vector of the interaction parameters (aerodynamic and aeroelastic parameters); $P(DS_j|EDP)$ is the structural fragility curve (i.e. the complementary cumulative distribution function of DS_j conditional on the occurrence of EDP); $f(EDP|IM, SP, IP)$ is the probability density function (PDF) of EDP conditional on IM, SP and IP; $f(IP|IM, SP)$ are the joint PDFs of the IP components conditional on IM and SP, $f[IM(\delta)]$ are the joint PDFs of the components of the intensity measure vector as a function of the building orientation angle δ and $f(SP)$ are the joint PDFs of the components of the vector SP.

Since most uncertainty is usually concentrated in the experimentally-

derived wind load [e.g. (Cui and Caracoglia, 2015)], the main uncertain quantities are the mean reference wind velocity V_{ref} referenced at the building top floor and corresponding to ten-minute averaging time at full scale (Figure 1), and the mean-wind direction measured from the North direction as defined in Eq. (5). The integration is carried out considering the mean-wind direction angle $(\theta + \delta)$ as the integration variable, noting that $\mathrm{d}(\theta + \delta) = \mathrm{d}\theta$.

Therefore, without loss of generality, the random elements of the intensity measure vector IM are V_{ref} and $(\theta + \delta)$. The joint PDF of the intensity measure vector is designated as $f(V_{ref}, \theta + \delta)$ and it refers to the mean-wind direction angle. The vector of interaction parameters IP is composed of the aerodynamic coefficients, i.e. determined from the pressure coefficients measured in the wind tunnel.

Assuming without loss of generality that SP are deterministic and that the randomness of IP is taken into account as explained in Section 2.1, the convolution integral in Eq. (6) becomes:

$$P_j^k(\delta) = \int\int\int P[DS_j|EDP(\theta)]f[EDP|V_{ref}, \theta] \\ f(V_{ref}, \theta + \delta)\mathrm{d}(EDP)\mathrm{d}(V_{ref})\mathrm{d}(\theta) \quad (7)$$

It is worth observing that, in the presence of a prevailing wind direction, the joint PDF of the IM vector, $f(V_{ref}, \theta + \delta)$ accounts for the building orientation angle δ. Moreover, the parameter EDP only depends on the relative mean-wind incidence angle θ since the structural analysis is conducted in accordance with the local coordinate system x, y.

2.4. Cost analysis

The cost analysis evaluates the total expected *repair and intervention* costs over a time period t corresponding to the lifetime of a structure. Without loss of generality, the ordinary maintenance and structural replacement costs are neglected, as well as the indirect business losses associated with activity interruption. The expected cost evaluation is based on the assumption that the structure is restored to its original condition after each occurrence of the wind-induced damage. For the sake of simplicity and as a first approximation in the absence of more-detailed design plans, the initial construction cost C_0 is assumed to be independent of the building orientation angle δ.

The total expected total life-cycle cost is computed as the sum of the initial cost C_0 (deterministic) and the expected repair costs in each k direction (Wen, 2001; Wen and Kang, 2001):

$$E[C^k(t,\delta)] = C_0 + E[\sum_{l=1}^{L}\sum_{j=1}^{K} C_j^k e^{-\lambda t_l} P_j^k(\delta)] \tag{8}$$

In the previous equation $E[.]$ denotes expected value; l is the loading occurrence number; L is the total number of loading occurrences between time 0 and time t; j is the damage state number; K is the total number of damage states under consideration; C_j^k is the cost of j^{th} damage state being reached in the k direction supposed as a deterministic quantity; λ is the discount rate per year; t_l is the loading occurrence time assumed as a uniform Poisson process. Ordinary maintenance costs are also excluded from the previous equation. The quantity $P_j^k(\delta)$ is the probability of exceeding the j^{th} damage state given the mean arrival rate ν per unit time (i.e., number of

events per year) (Mitropoulou et al., 2011) for a given building orientation δ:

$$P_j^k(\delta) = -\frac{1}{\nu t} log[1 - P_{tj}^k(\delta)] \tag{9}$$

where P_{tj}^k is the t-year probability of exceeding the damage state in the k direction, defined as follows:

$$P_{tj}^k(\delta) = 1 - [1 - P_j^k(\delta)]^t \tag{10}$$

where $P_j^k(\delta)$ is the annual damage probability evaluated through damage analysis, as explained in the previous Section 2.3.

Considering Eq. (9) and Eq. (10), a simplification is introduced below [Eq. (11)], which evaluates the expected value of the relative intervention and repair cost $c^k(t, \delta)$ normalized with respect to the initial construction cost C_0. The monetary variable $c^k(t, \delta)$ represents the portion of the lifetime cost that is directly connected to the repair and maintenance induced by wind damage in the k direction and, contrary to other cost items, is a function of the building orientation δ. Consequently, the variable $c^k(t, \delta)$ is exclusively needed by the minimization and optimization procedure to determine the optimal orientation. The quantity $c^k(t, \delta)$ is:

$$c^k(t, \delta) = E[\frac{C^k(t, \delta) - C_0}{C_0}] = E[\sum_{l=1}^{L} \sum_{j=1}^{K} c_j^k e^{-\lambda t_l} [-\frac{1}{\nu t} log(1 - P_{tj}^k(\delta))] \tag{11}$$

where $c_j^k = C_j^k / C_0$ is the normalized cost of the j^{th} damage state in the k direction. In the previous equation the probability of exceeding the j^{th} damage state, given the l^{th} occurrence of the hazard, is assumed to be invariant with time. The total expected normalized intervention and repair cost during the lifetime of the structure is evaluated as the summation of

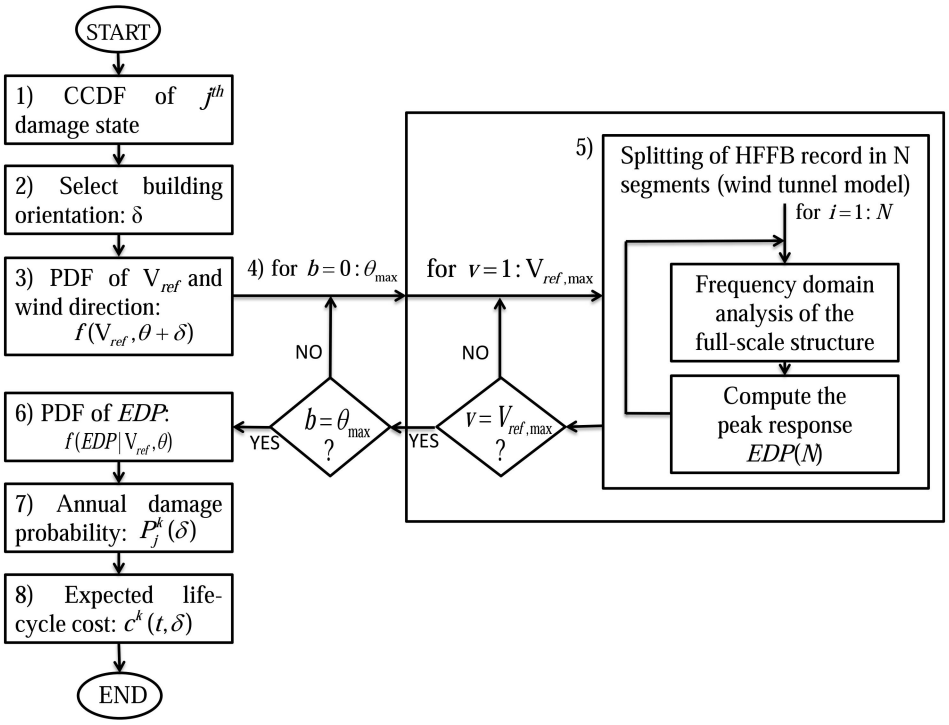

Figure 2: Flow chart of the proposed LCCA procedure.

the expected costs accounting for damage in all non-structural elements of the façade along the two main directions of the building. As above-outlined, since ordinary maintenance cost and construction cost are not affected by the hazard and damage occurrence, they are not included in the numerical results presented in the next sections.

2.5. The proposed LCCA algorithm

A flow chart of the multi-hazard life-cycle cost analysis procedure is illustrated in Figure 2.

The numerical procedure to evaluate the life-cycle monetary loss can be

summarized as follows:

1. Select the damage state j and evaluate the corresponding complementary cumulative distribution function, $P[DS_j|EDP]$ in Eq. (7);
2. Select the building orientation δ;
3. Evaluate the joint PDF of the reference mean-wind speed (V_{ref}) and wind direction (θ), $f(V_{ref}, \theta + \delta)$, for the specific site of the building;
4. Set the relative mean-wind incidence angle (θ) and the hazard (V_{ref}) intervals;
5. Evaluate the peak response [Eq. (17)] and the corresponding value of the selected EDP parameters from each one of the N segments of wind tunnel data and for each relative mean-wind incidence angle θ;
6. Assess the PDFs $f[EDP|V_{ref}, \theta]$ from the peak response values, independently computed using the N wind tunnel data segments;
7. Compute the annual damage probability through Eq. (7);
8. Assess the expected life-cycle cost as in Eq. (11);
9. Repeat steps $2 - 8$ for each direction δ.

3. Case study: wind load model and structural analysis

3.1. Description of the model

The benchmark case study is a reinforced-concrete tall building, 180 m high, with a rectangular floor plan (cross section) characterized by a side ratio $B/D = 1 : 1.5$ (Figure 3). A grid of 25 columns, equally distributed along the external perimeter, is placed in correspondence of each floor. The columns are made of concrete-filled steel tubes of variable dimension along

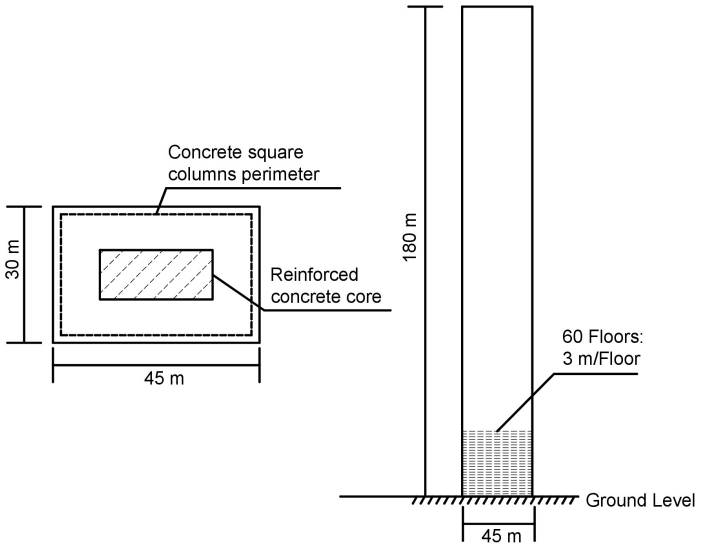

Figure 3: Schematic view of the 60-story building.

the building height. The main wind force resisting system is composed of the perimeter columns, central core, beams and cross-bracing in both directions.

3.2. Wind load model

The aerodynamic loads are obtained from measurements on a scaled model of the building, tested in the boundary layer wind tunnel at the Inter-University Research Center for Building Aerodynamics and Wind Engineering (CRIACIV), Prato, Italy. A suburban terrain wind speed profile (boundary layer described by a power-law model with exponent approximately equal to 0.23) is used to numerically simulate the experimental conditions. Tests are conducted on the rigid model of the benchmark building (geometric scale 1:500) at various mean-wind directions between 0° and 360° with 22.5° step increments. The base moments, proportional to the general-

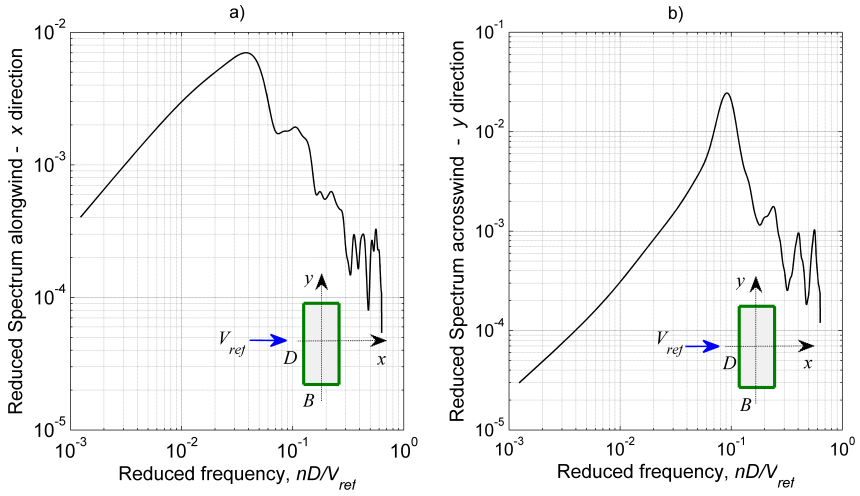

Figure 4: A realization of the generalized force spectrum [Eq. (3)], experimentally measured for $(\theta + \delta) = 0°$.

ized loads (Holmes, 1987), defined in Eq. (2), are determined by integrating pressure time histories over a set of 120 taps, 30 taps on each vertical face, equally divided into 5 levels. As explained in a previous section, a key point of the approach is the estimation of the uncertainties related to wind tunnel measurements.

To account for measurement variability, the 30 s long wind tunnel pressure records are divided in 8 segments, having a duration corresponding to ten minutes at full scale Each segment is treated as an independent realization of the generalized force, from which the structural response is independently evaluated. Figures 4a) and 4b) respectively illustrate two realizations of the normalized generalized force power spectra (PSDs) in the x and y directions as a function of the reduced frequency, at $(\theta + \delta = 0°)$.

The wind climate of the city of Boston, located in Massachusetts along

the Atlantic coast of the United States, is chosen as the site of the full-scale benchmark application in the numerical simulations. Boston is predominantly affected by extra-tropical synoptic winds and extremely rare hurricane events. In order to evaluate the influence of the mean-wind speed and direction, meteorological measurements available from an online database are used (NERACOOS). The data, recorded at the Station 44029 - Buoy A01 located in the Massachusetts Bay, are extracted from January 2001 to December 2016 and used to construct the PDF of θ (mean wind direction). The mean wind speeds, extracted from the records, are employed to examine the correlation between mean wind speed and direction. In fact, as described in Section 2.3, the vector IM depends on two positive real-valued random variables: the mean reference wind speed V_{ref} and the relative wind incidence angle (angle of attack) θ.

First, the dependence between mean-wind speed and mean-wind direction θ is examined; the correlation coefficient is evaluated from the sample of the random variables, extracted from Buoy A01. Since the sample correlation is equal to 0.0948, the two random variables can be considered, as a first approximation, as uncorrelated. Therefore, the term $f(V_{ref}, \theta+\delta)$ of Eq. (7) can be simplified as $f(V_{ref}, \theta + \delta) = f(V_{ref})f(\theta + \delta)$. Consequently, the estimation of the PDFs of mean-wind speed and direction can be carried out separately and Eq. (7) becomes:

$$P_j^k(\delta) = \int\int\int P[DS_j|EDP(\theta)]f[EDP|V_{ref}, \theta] \\ f(V_{ref})f(\theta + \delta)\mathrm{d}[EDP]\mathrm{d}(V_{ref})\mathrm{d}(\theta) \quad (12)$$

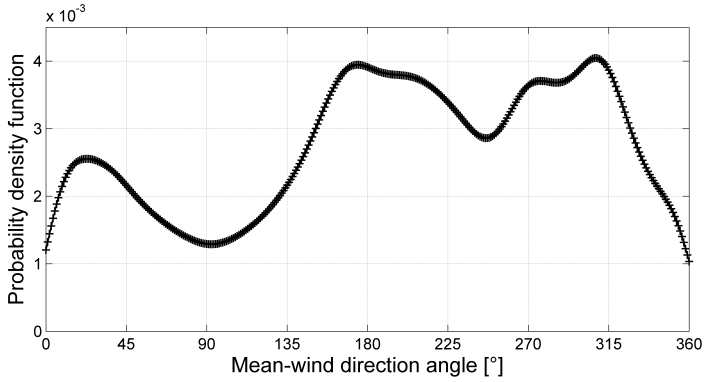

Figure 5: Empirical marginal distribution of the mean-wind direction derived from the database. The angles are measured from the North direction.

Therefore, the quantity $f(\theta + \delta)$ is determined as follows. Starting from the mean-wind direction with respect to the geographic North, taken from the database (NERACOOS), the experimental probability density function $f(\theta + \delta)$ of the mean-wind direction is evaluated (Figure 5). Since the probability distribution model is not known a priori, a non-parametric method is used to examine the data (Kernel density estimation) and derive a suitable PDF. The PDF in Figure 5 is multi-modal; the wind predominantly blows from the South-West quadrant and the North-West quadrant, confirming that the orientation of the building is a variable that cannot be neglected.

In contrast, a different approach is used to estimate the PDF of the yearly maxima of the mean-wind speed, necessary to derive the annual extreme wind speed PDF of V_{ref} at the reference roof-top elevation $f(V_{ref})$. The wind speeds recorded on the buoy are not used. Instead, the PDF is reconstructed from information provided in the United States design standard (ASCE7-16, 2017). The basic wind speeds (3-second gust at 10-meter elevation) of

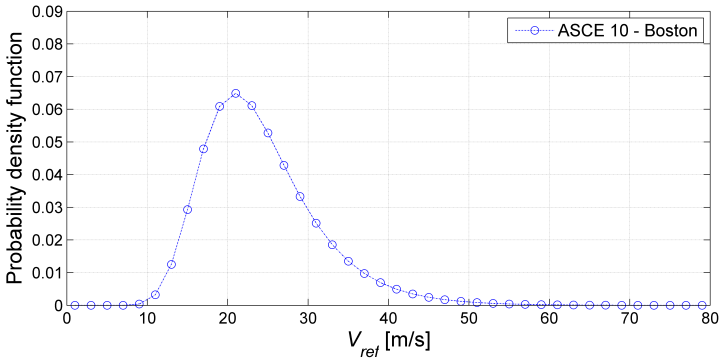

Figure 6: Probability density function of the mean-wind speed annual maxima (10-minute averaging time) at the reference elevation, $f(V_{ref})$.

the wind maps (exposure C category) are extracted for each return period; velocities are subsequently adjusted for averaging time (to 10-minute averages), change of exposure category (exposure B) and referenced to building's roof-top height (180 m) to get mean wind speeds V_{ref}. Exposure B category is employed since it is compatible with the mean wind speed profile used in the wind tunnel and representative of a suburban terrain roughness; the boundary layer is described by a power-law with exponent $\alpha = 0.25$. The resultant distribution function, which can be adequately represented by a Gumbel model, is plotted in Figure 6.

3.3. Structural fragility models for non-structural elements

Structural fragility curves are evaluated from the FEMA (Federal Emergency Management Agency) database, which is a protocol created for experimental research regarding the seismic performance characteristics of non-structural components (FEMA-P-58, 2012). The demand parameter or EDP

is the interstory drift ratio (IDR), derived from the maximum absolute value of the peak response at which damage occurs. Two specific drift-related damage states or levels are investigated in this study; they are illustrated in Figure 7: *in plane glass cracking* (D_1) and *glass falling from frame* (D_2). The curves in Figure 7 refer to a curtain wall system consisting of insulating glass components (dual panel). For the purpose of this discussion, the damage directly caused by the wind pressure load on the glass panels and by the water infiltration, is not directly included. Furthermore other damage probabilities (e.g. due to impact of wind-borne debris), are characterized by almost zero probability of occurrence in a non-hurricane climate area such as the one selected in this study; they are consequently neglected at this stage even though specific probability-based approaches for simple damage examination are available and could be readily included [e.g. Moghim and Caracoglia (2012)]. Without loss of generality, the present paper emphasizes the need for considering structural fragility curves, experimentally derived and readily available, in the proposed life-cycle cost design procedure. Because of the lack of experimental data for wind-induced damages, the seismic fragility curves, which are drift-related, are used. However the procedure could easily incorporate other types of damage of which experimental data are available.

4. Numerical simulation results

This section describes the main results of the numerical simulations for the estimation of the life-cycle monetary losses corresponding to the damage states D_1 and D_2.

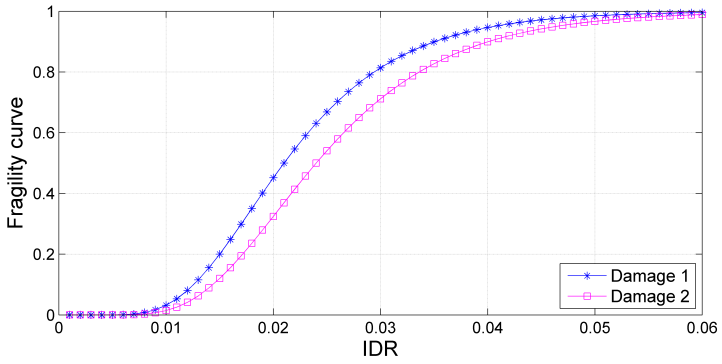

Figure 7: Damage 1 (D_1) and Damage 2 (D_2) fragility curves as a function of interstory drift ratio (IDR).

4.1. Limit-state and damage probability results

The uncertainties related to the experimental load are taken into consideration in the formulation by evaluating the term $f[EDP|V_{ref}, \theta]$ in Eq. (13), which represents the PDF of the selected EDP, i.e. the interstory drift ratio (IDR), conditional on the reference mean-wind speed, defined within each hazard intensity interval, on the relative mean-wind incidence angle θ and depending on building orientation.

As an example, Fig. 8a) presents the empirical probability density functions of the IDRs for three values of V_{ref} and plotted along with the corresponding D_2 fragility curve (Figure 7) for the x building direction and mean-wind incidence angle $(\theta + \delta) = 0^\circ$ (wind that blows from the North).

Figure 8b) illustrates the comparison between the numerical PDF, postulated from a log-normal distribution model, and the experimental PDF, found from the wind tunnel experimental loads by data parsing, at $V_{ref} = 50$ m/s. The close proximity between the interpolated probability curve and

the experimental points validates the adoption of the log-normal distribution model for the variable IDR. This choice possibly best fits the N peak responses, obtained from the corresponding N generalized fluctuating force spectra, which are evaluated by sampling the pressures and load time histories from the wind tunnel experiments.

In order to validate the LCCA procedure summarized in Sect. 2.5, some

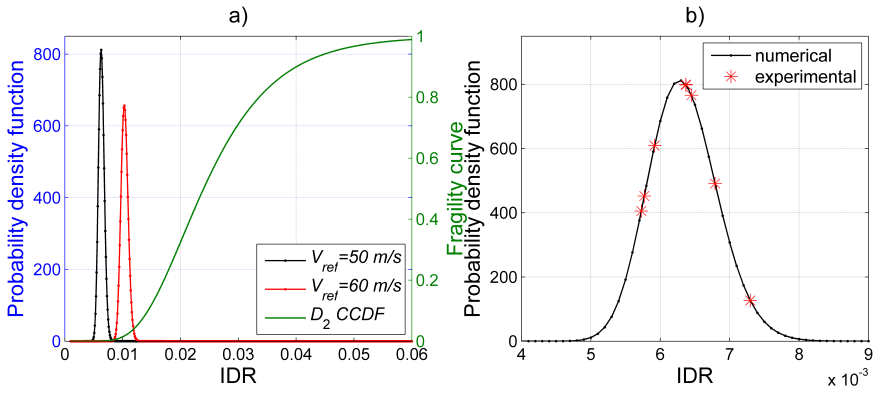

Figure 8: PDF(EDP) curves for direction x in the case of $(\theta + \delta = 0°)$: a) $f[EDP|V_{ref} = \{50, 60\}$ m/s] and D_2 fragility curve; b) numerical PDF, $f[EDP|V_{ref} = 50$ m/s], vs. experimental points.

intermediate results are computed. First, Figure 9 illustrates an example of top floor IDR associated with one of the N^{th} wind tunnel data segments for all relative incidence angles θ. As expected, the figure suggests the symmetry of the structural response in terms of IDR, given the rectangular floor plan of the building. Very small differences between symmetrical angles are possibly related to small experimental wind tunnel measurement inaccuracies. Furthermore, the prevailing effect of vortex shedding is noted when the relative incidence direction is orthogonal to the face of larger dimension (D),

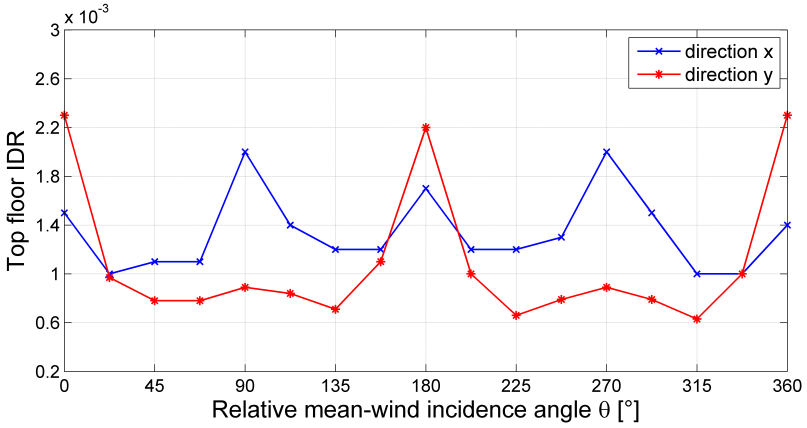

Figure 9: Peak top floor IDR for directions x, y (local coordinate system) with $V_{ref} = 40$ m/s as a function of the relative mean-wind incidence angle $0° \leq \theta < 360°$.

i.e. $\theta = \{0°, 360°\}$; in fact, the IDR exhibits a larger value in the direction y corresponding to the across-wind response. As explained earlier, it is convenient to decompose the calculation of the damage probability by separately considering each relative wind incidence angle θ. Using D_2 damage state as an example, the damage probability $P_2^k(\theta)$ is consequently evaluated as follows:

$$P_2^k(\theta) = \int \int P[DS_j|EDP(\theta)]f[EDP(\theta)|V_{ref}]f(V_{ref})d[EDP]\mathrm{d}(V_{ref}) \quad (13)$$

Inspection of the results in Figure 10 confirms the symmetry of the damage as well as already seen in the structural response with respect to θ. A considerable difference is noted between the damage along the two principal axes of the building, with higher annual damage probability values observed along the shorter side (principal building axis x) due to larger values of the associated IDR. Subsequently, the building orientation can be introduced and

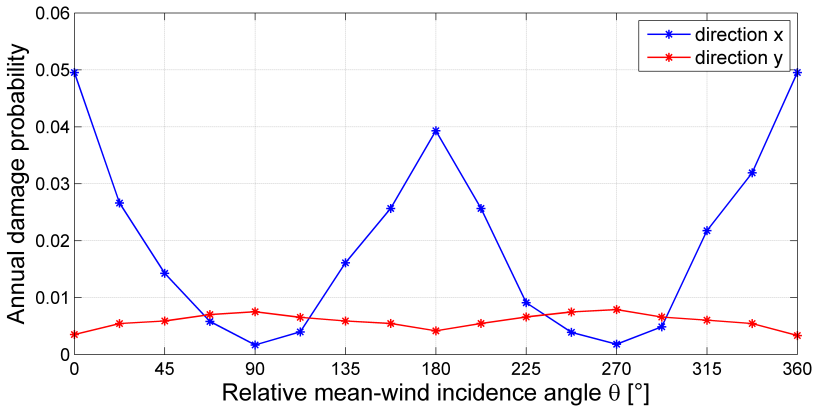

Figure 10: Annual damage probability P_2^k.

the annual damage probability is evaluated according to Eq. (13); results are plotted in the polar graphs of Figure 11.

From the examination of this figure, it is concluded that the annual damage probability is larger along the principal building axis x for both damage limit states. This is due to the fact that drift-dependent damage (Eq. 13) is more relevant for the x direction, as exhibited in Figure 9. Furthermore, the damage probability associated with the more severe damage limit state (D_2) in Figure 11b) is smaller for all δ, because of a rarer occurrence of very high winds.

4.2. Orientation-dependent damage cost accumulation results

The damage cost accumulation is assessed by simulating the number of wind storm events as a Poisson process between time 0 and the time t (in years). The arrival times of each storm, t_i, are simulated as uniformly distributed over the time interval by Monte-Carlo sampling. The parameters

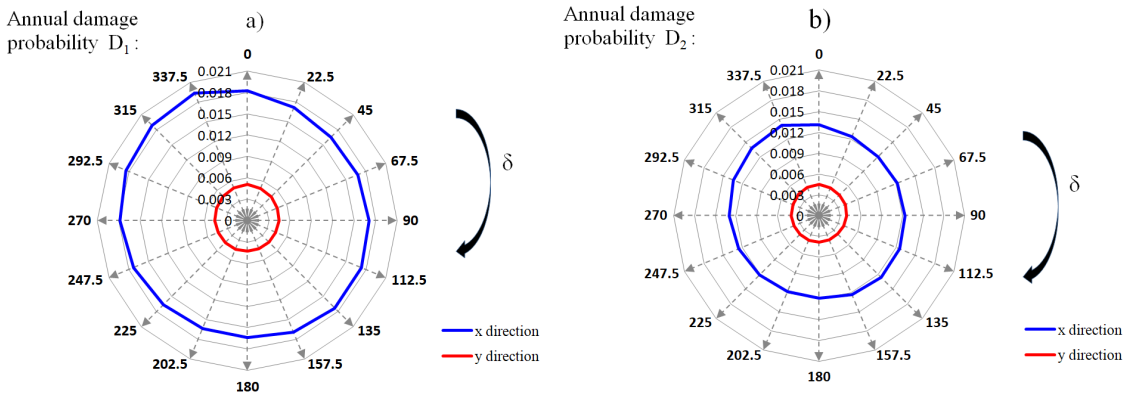

Figure 11: Annual damage probability as a function of building orientation δ (measured from the geographic North direction), $P_j^k(\delta)$: a) D_1 damage state; b) D_2 damage state.

that are employed for the cost analysis and described in Section 2.4, are summarized in Table 1 (Cui and Caracoglia, 2015); the same unit repair cost is used for both D_1 and D_2 and it is differentiated for the two main directions to take into account the side ratio of the building.

Figure 12 illustrates the numerical results of the cost analysis. The expected normalized annual intervention and repair costs (i.e. $t = 1$) is sepa-

Table 1: Parameters adopted for the cost analysis

PARAMETER		VALUE
Normalized unit repair cost x direction (c_1^x=c_2^x)	c^x	0.2
Normalized unit repair cost y direction (c_1^y=c_2^y)	c^y	$1.5 \cdot 0.2$
Mean arrival rate per unit time	ν	1
Discount factor	λ	0.05
Number of Monte-Carlo samples	N_s	10000

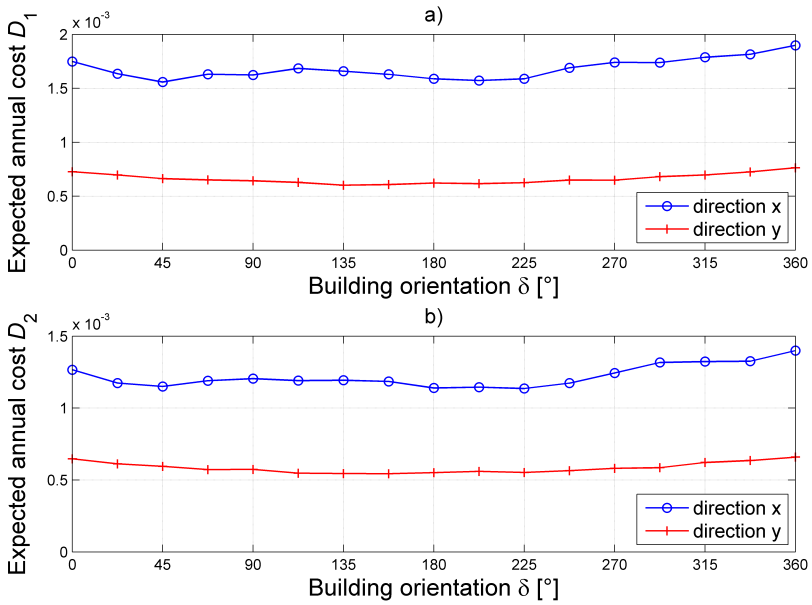

Figure 12: Expected value of the annual intervention and repair cost, normalized according to Eq. (11), along the two principal building axes: a) damage state D_1, b) damage state D_2.

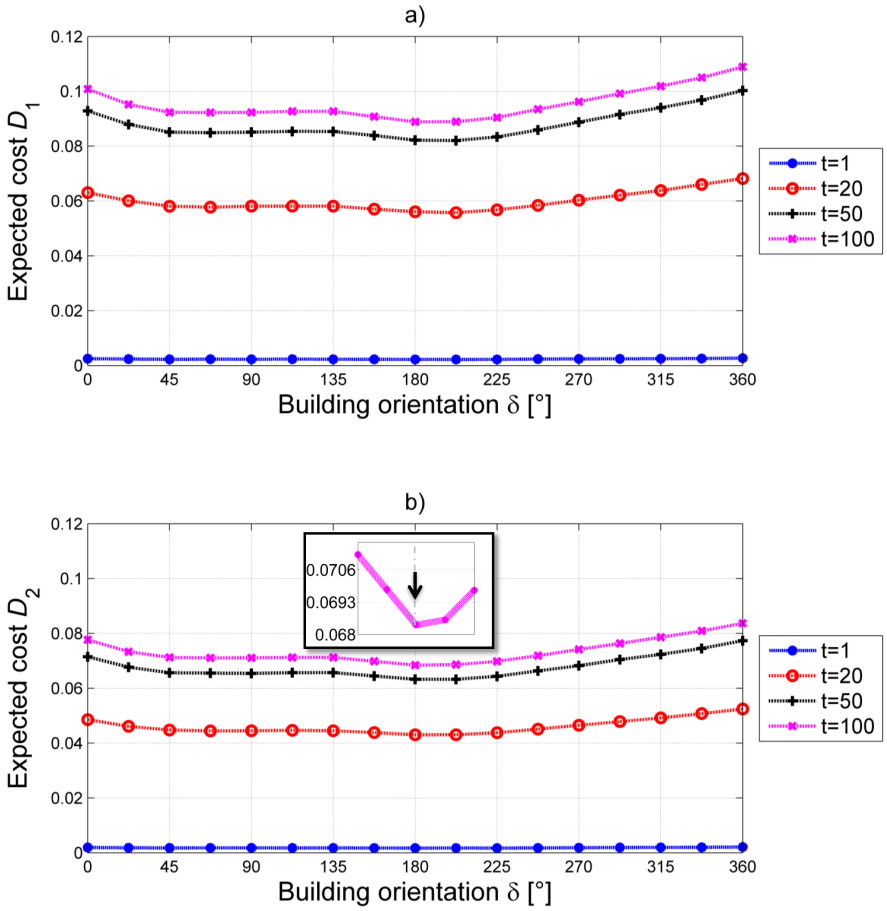

Figure 13: Expected total intervention and repair cost, normalized according to Eq. (11), as a function of the building orientation angle δ and for various lifetimes t (years): a) damage state D_1, b) damage state D_2, c) damage state D_2, t=100

rately presented for the two principal building axes (directions). Consistently with the damage analysis, larger damage probabilities along the x principal axis induce higher values of expected intervention and repair cost and more significant variations depending on the building orientation angle δ. Furthermore, since lower-intensity damage state (D_1) has a higher occurrence probability, the intervention and repair cost is greater in comparison with the cost associated with higher-intensity damage state (D_2).

In order to determine the best building orientation, the total combined cost is evaluated by cumulating the effects in the x and y directions. Figure 13 illustrates the total normalized intervention and repair cost, cumulating the costs along both building axes, for various lifetimes (return periods in years): 1, 20, 50, 100. As expected, the cost increases with time even though the curves maintain the same shape as a function of building orientation angle δ, according to Eq. (11). Inspection of this figure suggests that larger cost is related to lower-intensity damage state, which has a higher occurrence probability.

For both damage states and the specific case study, it is quite clear that the total expected cost has a minimum value at $\delta = 180^\circ$ as confirmed in the zoomed graph in Figure 13b). This result clearly depends on the selection of the geographical location and, consequently, on the wind exposure of the site, which is influenced by the empirical reconstruction of the probability density function of the mean-wind direction. The cost variations observed in the previous figures are influenced by the relative differences in the damage probability, which in turn depend on δ and the empirical PDF of the mean-wind direction, $f(\theta+\delta)$ in Eq. (13). The importance of the choice of the best

Table 2: Relative difference between minimum and maximum intervention and repair cost defined in Eq. (14).

Damage state	$t = 1$ year	$t = 20$ years	$t = 50$ years	$t = 100$ years
D_1	0.21	0.22	0.22	0.23
D_2	0.22	0.22	0.22	0.22

orientation is confirmed by the examination of Table 2, in which the relative difference between the minimum and maximum total intervention and repair cost is calculated for various lifetimes (return periods) t from:

$$\begin{cases} c_{\min}(t) = \min\limits_{\delta \in [0°, 360°)} \{c(t, \delta)\}] \\ c_{\max}(t) = \max\limits_{\delta \in [0°, 360°)} \{c(t, \delta)\}] \end{cases} \tag{14}$$

with $t = \{1, 20, 50, 100\}$ years. The relatives differences are significant and remain constant for each damage level, confirming that the orientation of the building is an important design parameter.

5. Preliminary analysis on the torsional effects

This section highlights the preliminary results of the numerical simulations by considering the influence of the torsional response in the LCCA. Indeed under the action of particularly strong wind events, a high-rise building can experience at the same time vibrations in the alongwind, acrosswind and torsional directions (Kareem and Zhou, 2003). In this context, the torsional rotation ψ is introduced in the schematic plan view of the case study building (Figure 14).

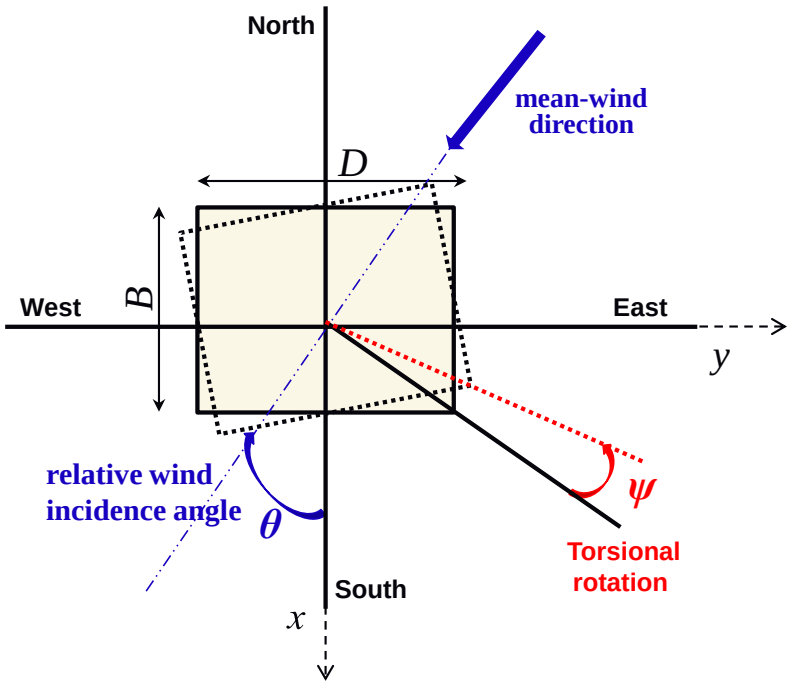

Figure 14: Schematic plan view of the building considering the torsional rotation ψ.

Apply the frequency domain analysis with the simplified hypothesis of uncoupled and linear principles vibrations modes (x, y, z), the i^{th} generalized torsional force $T_{Q_{i,k}}(t)$ in the k direction can be defined:

$$T_{Q_{i,k}}(t) = \int_0^H f_{i,k}^T(z,t)[\Phi_k(z)]\mathrm{d}z \tag{15}$$

where $f_{i,k}^T(z,t)$ is the i^{th} realization of the aerodynamic floor torque in the k direction. For the spectral analysis a correction factor $\mu = 0.33$ (Holmes et al., 2003; Tallin and Ellingwood, 1985) is used to correctly adjust the experimental evaluation of the uniformly distributed base torque along the height. The normalized power torque spectral density, shown in Figure 15 at $(\theta + \delta = 0°)$, is defined as follows:

$$nS_{\hat{T}_{Q_{i,k}}}(n) = \mu \cdot \frac{nS_{T_{Q_{i,k}}}(n)}{(1/2\rho V_{ref}^2 H D^2)^2} \tag{16}$$

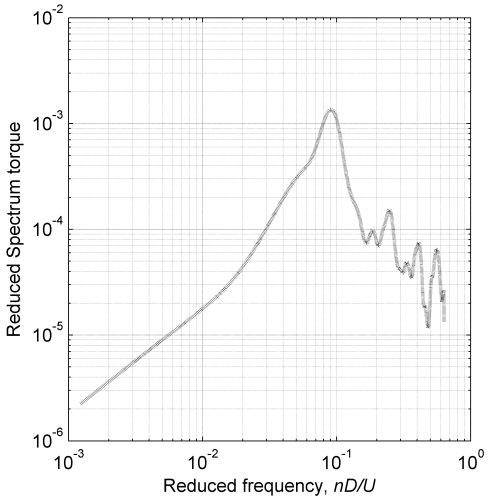

Figure 15: Reduced torque spectrum.

where n is the frequency and $S_{T_{Q_{i,k}}}$ is the power spectrum of the i^{th} experimental realization of the torque generalized force in the k^{th} direction.

The maximum lateral displacement $D_{n,i,k}$ of the structure in the k^{th} lateral direction of the building, for the i^{th} wind tunnel realization of the load, is specialized for each f^{th} side of the façade ($f = 1 : 4$) in order to consider the torsional effects:

$$D_{f,i,k} = (\bar{D}_{i,k} + \bar{D}^T_{f,i,k}) + \sqrt{(g_{i,k} \cdot \sigma_{D,i,k})^2 + (g^T_{f,i,k} \cdot \sigma^T_{D,f,i,k})^2} \qquad (17)$$

where $\bar{D}_{i,k}$, $\sigma_{D,i,k}$, $g_{i,k}$ are described in Section 3 and $\bar{D}^T_{f,i,k}$ is the torque mean response projected in the k direction, $\sigma^T_{D,f,i,k}$ is the standard deviation, $g^T_{f,i,k}$ is the Davenport's peak factor. For the sake of clarity a schematic representation of the torque-induced lateral mean displacements is shown in

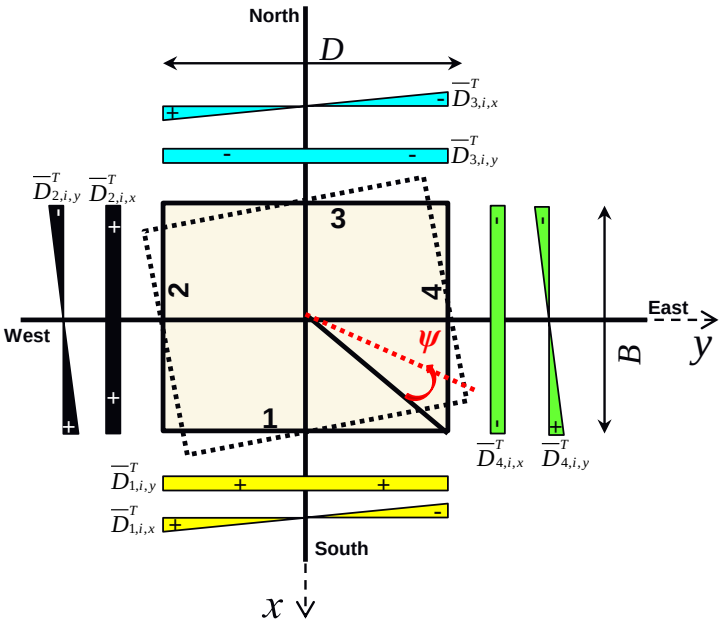

Figure 16: Torque-induced lateral displacements distributed along each side of the façade.

Figure 16. Since the IDR is the main EDP parameter chosen for the LCCA, only the in-plane displacements, which are constant in each side of the façade, are considered.

According to Equation 13 the annual damage probability for each side of the façade is evaluated. Results are compared (Figure 17) with those reported in Figure 10 in order to emphasize the influence of the torsional effects. As shown in the picture, the torsional response provokes a slight increase in terms of annual damage probability while it does not affect the best orientation of the building due to the similar distribution with respect to the mean-wind incidence angle. Hence higher values of the life cycle cost in time are expected.

6. Conclusions

In this paper a probability-based loss estimation model for wind-excited tall buildings is proposed, aimed at evaluating expected intervention and repair cost over the lifetime of the structure. The procedure considers the

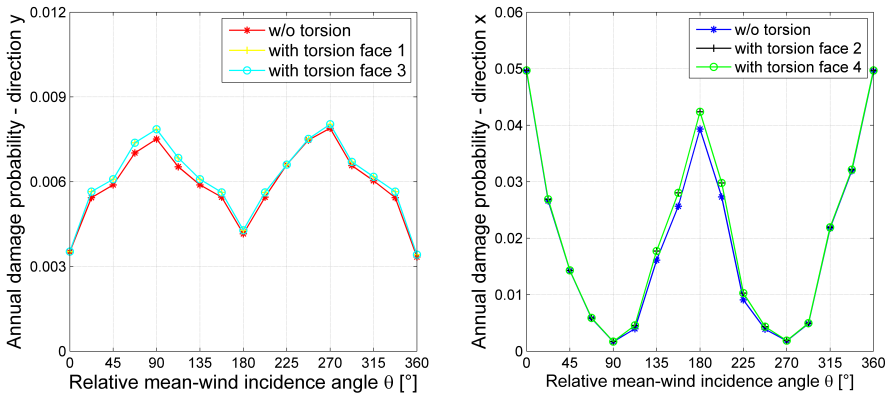

Figure 17: Annual damage probability including torsion (note: vertical-axis scales are different in the two panels to better present local variations).

uncertainties in wind load intensity and direction and accounts for the building's orientation relative to the prevailing wind directions.

A 180-meter tall rectangular floor-pan building is selected as the benchmark application problem. Uncertainties associated with the experimental assessment of the wind loads are considered by parsing the HFFB-based load spectra, evaluated from a wind tunnel test on a scaled model of the full-scale structure. In order to minimize the computational effort, wind tunnel records are directly converted to generalized forces, enabling the analysis in the frequency domain. Empirical structural fragility curves are selected from the FEMA seismic database. Damage to non-structural elements of the façade are considered in this first application example but the procedure could easily incorporate other types of damage. In order to evaluate the influence of the orientation of the tall building, the empirical probability density functions of the annual maxima of wind speed and direction is numerically reconstructed

by processing the data of an online database NERACOOS.

The approach emphasizes the importance of suitably selecting the structural fragility information and the relevance of carefully considering the wind exposure of the site. The use of the proposed procedure can provide useful information to the designer for choosing the building's orientation, which minimizes the total life-cycle cost. With the future challenge of including the damage states that mostly affect non-structural elements of wind-sensitive high-rise building structures, the proposed methodology offers an attractive approach for optimizing the design of tall buildings, improving their safety and performance while simultaneously reducing intervention costs over the years.

Acknowledgments

This research and the study period of Laura Ierimonti at Northeastern University in 2016 have been supported by the University of Perugia, Italy in the framework of the International PhD program between the Universities of Perugia, Florence and TU Braunschweig.

Luca Caracoglia would like to acknowledge the support of the National Science Foundation (NSF) of the United States, CAREER Award CMMI-0844977 in 2009-2014, and the partial support of NSF Award CMMI-1434880. Luca Caracoglia also acknowledges the support of the University of Perugia, mobility program for visiting professors in 2015. Any opinions, findings and conclusions or recommendations are those of the authors and do not necessarily reflect the views of the sponsors.

References

ASCE7-16, 2017. Minimum Design Loads for Buildings and Other Structures. American Society of Civil Engineers, Reston, Virginia (USA).

Aslani, H., Miranda, E., 2005. Probabilistic earthquake loss estimation and loss disaggregation in buildings, Report No. 157, in: The John A. Blume Earthquake Engineering Center. Stanford University, Stanford, California (USA).

Beck, A., Kougioumtzoglou, I., dos Santos, K., 2014. Optimal performance-based design of non-linear stochastic dynamical RC structures subject to stationary wind excitation. Engineering Structures 78, 145–53.

Caracoglia, L., 2014. A stochastic model for examining along-wind loading uncertainty and intervention costs due to wind-induced damage on tall buildings. Engineering Structures 78, 121–32.

Charney, F., Johnson, R., 1986. The effect of panel zone deformation on the drift of steel-framed structures, in: Proceedings of the ASCE Structures Congress, New Orleans, LA.

Ciampoli, M., Petrini, F., 2012. Performance-based aeolian risk assessment and reduction for tall buildings. Probabilistic Engineering Mechanics 28, 75–84.

Ciampoli, M., Petrini, F., Augusti, G., 2011. Performance-based wind engineering: towards a general procedure. Structural Safety 32, 367–78.

Cornell, C., Krawinkler, H., 2000. Progress and challenges in seismic performance assessment. PEER Center News 3, 1–3.

Cui, W., Caracoglia, L., 2015. Simulation and analysis of intervention costs due to wind-induced damage on tall building. Engineering Structures 87, 183–97.

Cui, W., Caracoglia, L., 2016. Exploring hurricane wind speed along US atlantic coast in warming climate and effects on predictions of structural damage and intervention costs. Engineering Structures 112, 209–25.

Davenport, A.G., 1964. Note on the distribution of the largest value of a random function with application to gust loading. Proceeding of the Institutions of civili Engineering 28, 187–96.

FEMA-P-58, 2012. Seismic Performance Assessment of Building, Volume 3. Technical Report. URL: http://www.fema.gov/media-library/assets/documents/90380.

Griffis, L., 1993. Serviceability limit states under wind load. Engineering Journal AISC .

Holmes, J., 1987. Extreme wind speeds in mixed climates revisited. Engineering Structures 9, 210–2.

Holmes, J., Rofail, A., Aurelius, L., 2003. High frequency base balance methodologies for tall buildings with torsional and coupled resonant modes, in: Proceedings of the 11^{th} International Conference on Wind Engineering, Lubbock, USA. pp. 2381–8.

Huang, M., Li, Q., Chan, C., Lou, W., Kwok, K., Li, G., 2016. Performance-based design optimization of tall concrete framed structures subject to wind excitations. Journal of Wind Engineering and Industrial Aerodynamics 139, 70–81.

Jain, A., Srinivasan, M., Hart, G., 2001. Performance based design extreme wind loads on a tall building. The structural design of tall buildings 10, 9–26.

Kareem, A., Zhou, Y., 2003. Gust loading factor - past, present and future. Journal of Wind Engineering and Industrial Aerodynamics 91, 1301–28. doi:10.1016/j.jweia.2003.09.003.

LaFave, J., Gao, Z., Holder, D., Kuo, M., Fahnestock, L., 2016. Commercial and residential building performance during the May 20, 2013, Tornado in Moore, Oklahoma. Journal of Performance of Constructed Facilities 30, 04014210.

Lagaros, N., 2007. Life-cycle cost analysis of design practices for RC framed structures. Bulletin of Earthquake Engineering 5, 425–42.

Li, G., Hu, H., 2014. Risk design optimization using many-objective evolutionary algorithm with application to performance-based wind engineering of tall buildings. Structural Safety 48, 1–14.

Liu, M., Wen, Y., Burns, S., 2004. Life cycle cost oriented seismic design optimization of steel moment frame structures with risk-taking preference. Engineering Structures 26, 1407–21.

Mitropoulou, C., Lagaros, N., Papadrakakis, M., 2011. Life-cycle cost assessment of optimally designed reinforced concrete buildings under seismic actions. Reliability Engineering and System Safety 96, 1311–31.

Moghim, F., Caracoglia, L., 2012. A numerical model for wind-borne compact debris trajectory estimation: part 1 – probabilistic analysis of trajectory in the proximity of tall buildings. Engineering Structures 38, 153–62.

NERACOOS, . Northeastern Regional Association of Coastal and Ocean Observing Systems. Technical Report. URL: `http://www.neracoos.org/`.

Okasha, N., Frangopol, D., 2011. Computational platform for the integrated life-cycle management of highway bridges. Engineering Structures 33, 2145–53.

PEER-TBI, 2010. Tall Buildings Initiative, Guidelines for performance-based seismic design of tall buildings. Report No. 2010/05. TBI Guidelines Working Group. Pacific Earthquake Engineering Research Center, University of Berkeley, Berkeley, California (USA).

Pozzuoli, C., Bartoli, G., Peil, U., Clobes, M., 2013. Serviceability wind risk assessment of tall buildings including aerolastic effects. Journal of Wind Engineering and Industrial Aerodynamics 123, 325–38.

Ramirez, C., Liel, A., Mitrani-Reiser, J., Haselton, C., Spear, A., Steiner, J., G.G., D., E., M., 2012. Expected earthquake damage and repair costs in reinforced concrete frame buildings. Earthquake Engineering and Structural Dynamics 41, 1455–75.

Ramirez, C., Miranda, E., 2012. Significance of residual drifts in building earthquake loss estimation. Earthquake Engineering and Structural Dynamics 41, 1477–93.

Seo, D., Caracoglia, L., 2013. Estimating life-cycle monetary losses due to wind hazards: Fragility analysis of long-span bridges. Engineering Structures 56, 1593–606.

Spence, S., Kareem, A., 2014. Performance-based design and optimization of uncertain wind-excited dynamic building systems. Engineering Structures 78, 133–44.

Tallin, A., Ellingwood, B., 1985. Analysis of torsional moments on tall buildings. Journal of Wind Engineering and Industrial Aerodynamics 18, 191–5. doi:10.1016/0167-6105(85)90097-2.

Venanzi, I., 2015. Robust optimal design of tuned mass dampers for tall buildings with uncertain parameters. Structural and Multidisciplinary Optimization 51, 239–50.

Venanzi, I., Lavan, O., Fabrizi, S., 2017. Multi-hazard life-cycle performance of tall buildings under seismic and wind loads, in: Life-Cycle of Engineering Systems: Emphasis on Sustainable Civil Infrastructure - 5th International Symposium on Life-Cycle Engineering, IALCCE 2016, pp. 177–84.

Venanzi, I., Materazzi, A., Ierimonti, L., 2015. Robust and reliable optimization of wind-excited cable-stayed masts. Journal of Wind Engineering and Industrial Aerodynamics 147, 368–79.

Venanzi, I., Salciarini, D., Tamagnini, C., 2014. The effect of soil-foundation-structure interaction on the wind-induced response of tall buildings. Engineering Structures 79, 117–30.

Wang, L., Zhao, X., Zheng, Y., 2016. A combined tuned damper and an optimal design method for wind-induced vibration control for super tall buildings. Structural Design of Tall and Special Buildings 25, 468–502.

Wen, Y., 2001. Minimum lifecycle cost design under multiple hazards. Reliability Engineering and System Safety 73, 223–31.

Wen, Y., Kang, Y., 2001. Minimum building life-cycle cost design criteria. i: Methodology. Journal of Structural Engineering, ASCE 127, 330–7.